Low-Energy Energetic Neutral Atom Imaging of Io Plasma and Neutral Tori

Yoshifumi Futaana, Stas Barabash, Xiao-Dong Wang, Martin Wieser, and Gabriella S. Wieser

Swedish Institute of Space Physics, Box 812, Kiruna 98128, Sweden.

Peter Wurz

University of Bern.

Norbert Krupp

Max Planck Institute for Solar System Research.

Pontus C:son Brandt

Applied Physics Laboratory, Johns Hopkins University.

Corresponding author

Yoshifumi Futaana, Swedish Institute of Space Physics, Box 812, Kiruna 98128, Sweden.

E-mail: futaana@irf.se
Tel: +46-980-79025
Fax: +46-980-79050

Abstract

Io's plasma and neutral tori play significant roles in the Jovian magnetosphere. We present feasibility studies of measuring low-energy energetic neutral atoms (LENAs) generated from the Io tori. We calculate the LENA flux between 10 eV and 3 keV. The energy range includes the corotational plasma flow energy. The expected differential flux at Ganymede distance is typically 10^3-10^5 cm^{-2} s^{-1} sr^{-1} eV^{-1} near the energy of the corotation. It is above the detection level of the planned LENA sensor that is to be flown to the Jupiter system with integration times of 0.01–1 seconds. The flux has strong asymmetry with respective to the Io phase. The observations will exhibit periodicities, which can be attributed to the Jovian magnetosphere rotation and the rotation of Io around Jupiter. The energy spectra will exhibit dispersion signatures, because of the non-negligible flight time of the LENAs from Io to the satellite. In 2030, the Jupiter exploration mission JUICE will conduct a LENA

measurement with a LENA instrument, the Jovian Neutrals Analyzer (JNA). From the LENA observations collected by JNA, we will be able to derive characteristic quantities, such as the density, velocity, velocity distribution function, and composition of plasma-torus particles. We also discuss the possible physics to be explored by JNA in addition to the constraints for operating the sensor and analyzing the obtained dataset.

1. Introduction

1.1 Io neutral and plasma tori

Io, the innermost Galilean moon of Jupiter, introduces a large amount material of volcanic origin to the Jovian magnetosphere. As a result, the Jovian magnetosphere is composed of heavy ions (oxygen, sulfur, and their compounds). The strong and localized source of particles near Io creates characteristic spatial distributions of plasma and neutral particles in the Jovian magnetosphere, namely, the Io neutral and plasma tori (see, for example, reviews by Dessler 1983; Thomas et al. 2004; Schneider and Bagenal, 2007; and references therein).

The Io neutral torus (called also as neutral cloud) is a dense concentration of atoms and molecules of volcanic origin that has formed around the Io orbit. These atoms are gravitationally bound to Jupiter. The composition is mainly sulfur (S) and oxygen (O) atoms as well as their compounds (e.g. Thomas et al., 2004). Hydrogen (H) atoms also exist, but the fraction thereof is small. Sodium (Na) atoms are also present. Na is bright because of its D-lines, but the fraction thereof is quite small; therefore the Na imaging is considered as a trace gas of more abundant compositions in the neutral torus (Mendillo et al., 2004). These atoms form a partial ring-like shape, which is associated with the short time scale of the loss of atoms via ionization (a few hours to 10s of hours depending on the processes; see e.g. Schneider and Bagenal., 2007) compared to the filling time of the full torus (~150 hours assuming 2.5 km/s, the escape velocity of Io).

When the neutral components in the Io neutral torus are ionized, the charged particles are accelerated by the motional electric field in the

corotational flow in the magnetosphere. The accelerated ions form a plasma torus. The main components are (singly or multiply) charged O ions and S ions. H^+ ions are also present but the fraction thereof is less abundant. It is often assumed 10% [e.g. Thomas et al. 2004]. However, there are several measurements showing much smaller fraction than 10% (e.g. Wang et al., 1998a, b; Zarka et al., 2001). The plasma in the torus is corotating with the Jovian magnetosphere. At the Io orbit, the corotational velocity of the plasma is ~74 km/s. The revolution speed of Io is ~17 km/s in the same direction as the corotational flow, so the relative plasma flow velocity is ~57 km/s (e.g. Thomas et al., 2004). Even though the plasma source is more localized, because of the longer residence time (Schneider and Bagenal, 2007) compared with the rotation of the Jovian magnetosphere (9.925 hour) the plasma torus is nearly axisymmetric in a plane, referred to as the centrifugal equator (Hill 1974), defined by the rotation and magnetic dipole tilt. The tilt of the magnetic dipole is ~9.6˚ (according to the so-called O4 model; Acuña and Ness, 1976), while that of the centrifugal equator is represented as 2/3 of the magnetic tilt (Hill 1974).

After the Io neutral torus was discovered via the D-line emission of Na (Brown 1974) and Io plasma torus via S+ emission (Kupo et al., 1976), many observations on Io tori have been performed. Historically, investigations of the Io tori have been conducted via UV and IR spectroscopy (Herbert et al., 2001; Mendillo et al, 2004; Nozawa et al., 2004; Steffl et al., 2004a; 2004b; 2006; 2008; Yoneda et al., 2010; 2014) and in situ plasma observations (Bagenal., 1994; 1997a; 1997b; Frank and Paterson, 2001). Attempts for understanding the characteristics and the dynamics of Iogenic particles inside the Jovian magnetosphere are not only driven by the interests in magnetospheric science, but also the Io tori directly associate with the Io's volcanic activities (e.g. Herbert et al., 2001; Mendillo et al., 2004, 2007; Nozawa et al., 2004; Yoneda et al., 2010; 2014). The recent developed technique of energetic neutral atom (ENA) imaging has the potential to provide information concerning the Io plasma and neutral tori in an efficient manner.

1.2 Energetic neutral atom imaging in Jovian system

ENA imaging is a technique for the remote investigation of the interaction between space plasma and neutrals (e.g. Roelof and Williams, 1988; Gruntmann, 1997). Several ENA instruments have been carried into space, and the data collected by these instruments have been used to study the interactions between space plasma and neutral gas (e.g. Burch, 2000, 2003; Krimigis et al., 2002; Mauk et al., 2003; Brandt et al., 2005; Futaana et al., 2011; Goldstein and McComas, 2013). More recently, ENA imaging has also been successfully applied to investigations of the interactions between space plasma and the Moon surface (e.g. Futaana et al., 2006; McComas et al., 2009; Wieser et al., 2009; Schaufelberger et al., 2011; Futaana et al., 2012).

ENAs near Jupiter were detected by the Voyager 1 low-energy charged particle (LECP) instrument. LECP is a sensor for high-energy plasma particles, (Krimigis et al., 1977) but Kirsch et al. (1981) concluded the energetic neutral atoms were a possible explanation of one of the observed signals. Cheng (1986) calculated the interaction between plasma and neutral atoms in the inner magnetosphere and concluded that the charge exchange makes a significant contribution to the fluxes of energetic neutral particles. Based on the dedicated ENA measurement performed by Cassini/INCA, Krimigis et al. (2002) reported the firm evidence of high-energy ENAs (HENAs; >10 keV) emitted from the Jupiter system. Later, Mauk et al. (2003) claimed that the observed ENAs in the range of 50–80 keV originated from a region slightly outside of the Europa orbit (trans-Europa gas tori).

These previous observations of ENAs in the Jupiter environment were only conducted in the high-energy regime (>10 keV). No low-energy ENA (LENA) instrument (with a typical energy range of 10 eV to a few keV) has been employed in the Jovian system, although there are some speculation for studying moon-plasma interactions [Plainaki et al., 2010; Mililo et al., 2013; Grasset et al., 2013]. This unexplored energy range of LENAs is expected to provide us with valuable information regarding the characteristics of the Io tori, their formation and loss mechanisms, and associated transport mechanisms of iogenic materials. Whereas a fraction of the energy is carried by high-energy particles in the Jovian system, the mass transfer, namely, the outward transport

of iogenic materials, is dominated by low-energy particles (Bagenal and Delamere, 2011). From this perspective, the low-energy particles are essential to the characterization of the Jovian plasma environment.

1.3 Low-energy Energetic Neutral Atom imaging

Several LENA instruments have been used to investigate extraterrestrial environments. For example, the Neutral Particle Imager and Neutral Particle Detector were placed on board European Space Agency's (ESA's) Mars Express to establish a basic understanding of the ENA environment of Mars (Barabash et al., 2006). Replicas of these detectors were flown to Venus on the Venus Express mission (Barabash et al., 2007). IBEX-Lo has imaged the heliopause from the Earth orbit (McComas et al., 2009). The Chandrayaan-1 Energetic Neutrals Analyzer (CENA) was placed into Moon orbit (e.g., Kazama et al., 2006; Barabash et al., 2009), providing evidence of interaction between the solar wind and regolith surface. A replica of CENA, named Energetic Neutrals Analyzer (ENA), will be flown to Mercury with the ESA-JAXA joint mission, BepiColombo as a part of Mercury Plasma Particle Experiment (MPPE) on the Mercury Magnetospheric Orbiter (MMO) spacecraft (Saito et al., 2010). BepiColombo will also carry another LENA sensor, as part of the Search for Exospheric Refilling and Emitted Neutral Abundances (SERENA) package, on the Mercury Planetary Orbiter (MPO) spacecraft (Orsini et al., 2010). These aim to image Mercury-plasma interaction by LENAs (e.g. Grande 1997; Barabash et al., 2001; Orsini et al., 2001; Massetti et al., 2003).

In 2022, ESA will launch its first Jupiter mission, JUpiter ICy moons Explorer (JUICE; Grasset et al., 2013). JUICE is equipped with a complete plasma package, Particle Environment Package (PEP), which includes a LENA sensor named Jovian Neutrals Analyzer (JNA). The measurement principle of JNA is identical to that of ENA and CENA (Kazama et al., 2006; Barabash et al., 2009).

In this paper, we estimate the LENA flux produced by charge-exchange reactions between particles in the Io neutral and plasma tori to demonstrate the feasibility of LENA observations from Ganymede orbit using existing LENA

sensors. We assume simple models of the plasma and neutral tori. There are several reasons for using the simple models; first, such models require only a relatively short computational time for iterative calculation of the densities and velocity distribution functions of plasma and neutral tori; second, the line-of-sight integration for the LENA calculation will obscure details of small structures in any case; and third, simple models provide morphologic pictures that are useful for examining the application of this new technique of the LENA imaging to unexplored environment. The model is static, although the Io plasma and neutral tori are known to have temporal variations (e.g. Frank and Paterson et al., 2001; Herbert et al., 2001; 2003; Delamere et al., 2004; Nozawa et al., 2004; Yoneda et al., 2009; Steffl et al., 2004a; 2006). This is because this paper aims to understand the characteristics of LENA flux, particularly its intrinsic variations of the LENA flux due to the measurement technique and its limitations. In section 4, environmental variations, which are important for understanding nature of the Io tori, will be discussed.

We calculate the LENA flux along the planned trajectory of the JUICE spacecraft (Grasset et al., 2013) and discuss the observation capabilities of JNA on board. In addition, we discuss the possible physics to be explored by JNA as well as the constraints for operating the sensor and analyzing the obtained dataset. We do not attempt to discuss the detailed physics of the Io tori in this paper.

2. Models

The primary generation mechanism of LENAs near the Io tori is charge-exchange (also called "charge transfer"). Because of the co-existence of ions and neutral atoms, ions in the plasma torus (X^{n+}), experience charge exchange with neutral atoms in the neutral torus (Y):

$$X^{n+} + Y \rightarrow X^{*} + Y^{n+}$$

After the charge exchange, a neutral atom (X^{*}; ENA) and an ion (Y^{n+}) are formed. The newly ionized particles begin to corotate. The newly born neutral atoms have nearly the same energy (e.g. Rees, 1989) as that of the primary ion, which corresponds to the corotational flow (~74 km/s at the Io orbit, or ~29

eV/amu, namely ~29 eV for H, ~460 eV for O, and ~920 eV for S). The energies of these atoms are in the LENA energy range.

To calculate the expected LENA flux, one must construct models of the plasma and neutral tori. In addition, the cross sections for the relevant charge-exchange reactions are required. From those models, we can derive the expected ENA fluxes using the following formulation.

$$f_{\mathrm{ENA}}(\vec{r_0}, \vec{v_0}; t=0) = \int_{-\infty}^{0} f_{\mathrm{plasma}}(\vec{r_1}, \vec{v_1}; t_1) \cdot \sigma \cdot N_n(\vec{r_1}, t1) dl$$

Here, f_{ENA} is the ENA flux at the spacecraft position $\vec{r}_0$ and with the velocity $\vec{v}_0$ at a certain time (t=0). The integral is taken from the spacecraft position back in time along the Kepler trajectory of the ENA. The distance along the trajectory is denoted by l. The plasma velocity distribution function f_{plasma} is calculated for the position $\vec{r}_1$ and velocity $\vec{v}_1$ at generation, which are also determined from the Keplerian motion. N_{n} is the neutral density, and σ is the charge-exchange cross section. Details of the formulation are described in Appendix A.

Several sophisticated neutral-torus models have been proposed, and some of them reflect the physics very precisely (e.g. Smyth, 1992; Wilson et al., 2002; Smyth and Marconi, 2003). However, based on a simplified approach, we constructed our neutral-torus model in an analytic form. We modeled the density as a sum of two exponential distributions:

$$n(R,\theta) = n_0 \exp\left(-\frac{|\theta|}{\theta_0} - \frac{|R|}{R_0}\right) + n_1 \exp\left(-\frac{|\theta|}{\theta_1} - \frac{|R|}{R_1}\right)$$

$$\theta_i = \begin{cases} \theta_{ih} & (\theta > 0) \\ \theta_{it} & (\theta < 0) \end{cases}$$

Here, $n(R, \theta)$ is the density at the distance R from the Io torus and the separation angle (θ) from the Jupiter-Io line and n_0 and n_1 is the number densities for each distribution. The parameters θ_0, θ_1, r_0, and r_1 define the spread of the distribution. Different θ_0 values are used to consider the asymmetry between the leading and trailing parts of the torus; namely, θ_{0h} is used for the leading part (θ>0), and θ_{0t} is used for the trailing part (θ<0). The assumed values are as follows: n_0 = 15000 cm^{-3}, R_0 = 0.072 Rj, θ_{0h} = 14.4°, θ_{0t} = 3.6°, n_1 = 50

223 cm^{-3}, R_1 = 0.72 Rj, θ_{0h} = 86.6˚, and θ_{0t} = 14.4˚. The typical density of the neutral
224 torus on a global scale is controlled by the second component (parameter n_1).
225 This value was selected to be very close to those used in previous studies, such
226 as Johnson and Strobel (1982) and Cheng (1986). Figure 1b compares the results
227 obtained using the simple model employed here and a numerical model
228 proposed by Smyth and Marconi (2003). Parameters in our simple model was
229 chosen to capture the general trend of the Io neutral torus. However, our model
230 underestimates the neutral density in most of the region. In some region, the
231 underestimation is by a factor of 10 or more. For our purpose of demonstrating
232 the feasibility of LENA imaging from Ganymede orbit, an underestimation of the
233 LENA flux is preferable rather than an overestimation. The neutral-torus model
234 does not include any composition (H, O or S) information. Although the neutral
235 composition only plays a key role to the amount of ENA via the cross section,
236 the composition information will be reflected into only the cross section model.
237 All neutral atoms are assumed to move at a speed that corresponds to Io's
238 orbital velocity.
239 For our plasma-torus model, the same argument for using a simple
240 analytical model is applied. In practice, the simplicity is of great benefit with
241 respect to the impact on computational resources because we need to calculate
242 the velocity distribution function of ions in the plasma torus (Appendix A). We
243 assumed the following model. The plasma-torus structure is independent of the
244 Io phase. Although there are a few models that better represent the Jovian
245 magnetosphere (e.g., Acuña and Ness, 1976; Dougherty et al., 1996; Connerney
246 et al., 1998), we employed a perfect dipole here. We used the dipole
247 component parameters from the O4 model, namely, the tilt of the dipole field is
248 9.6˚, pointing to the west longitude of 201.7˚ in the System III coordinate system
249 (Acuña and Ness, 1976). However, it is known that the central plane (peak
250 density along a magnetic field line) of the plasma torus is located at the
251 centrifugal equator (Hill, 1974; Bagenal and Sullivan, 1981), which is between
252 the Jovian equator plane and magnetic equator plane. The maximum separation
253 between the centrifugal equator and magnetic equator is ~3.2˚ (Hill, 1974).
254 Therefore, we assumed the tilt of dipole axis to be 6.4˚ to emulate the

centrifugal equator instead of using the actual tilt of ~9.6° above. Indeed, the change in the tilt angle of the dipole axis does not impact on the morphologic views of the following results.

The total density of plasma-torus ions at the magnetic equator, $n_L(r)$, was taken from Divine and Garrett (1983) but slightly simplified inside the Io distance (Figure 2b). Figure 2b also indicate values of other existing models: Bagenal (1994), based on Voyager 1 data later validated by Galileo data; and Bagenal and Delamere (2011) based on Galileo data. These models provide slightly higher values especially in the inner region, but anyway, less than a factor of 10 of the present model. Away from the equator, we modified the density by the scale height of H, $\exp(-z/H)^2$, adopting Hill and Michel (1976) and other authors (e.g. Bagenal et al., 1994; Bagenal and Delamere, 2011). Here, z is the distance from the centrifugal equator along the field line and H (Rj) is $0.64\times(\mathrm{Ti(eV)/Ai(amu)})^{1/2}$. We assumed the bulk plasma to flow azimuthally with the corotation velocity and the thermal speed, v_{th}, corresponding to 70 eV for all species (Kivelson et al., 2004). For O^+, this value corresponds to v_{th} ~5.5 km/s. The assumed temperature of 70 eV is slightly higher than the data obtained from Voyager 1 PLS and Galileo PLS by a factor of 2–3 (see Figure 3 in Beganel and Delamere, 2011), while the difference in thermal velocity is less significant (√2–√3). We assume that the velocity distribution function is an isotropic Maxwellian. This assumption significantly underestimates the high-energy portion of the velocity distribution.

We also require cross-section models for the charge-exchange reactions. There are three main neutral components (S, O, H, and their compounds) and their ions (S^{n+}, O^{n+}, and H^+). Table 1 provides a list of the expected charge-exchange cross sections (Johnson and Strobel, 1982; McGrath and Johnson, 1989) for a relative velocity of ~60 km/s. The typical cross section for charge exchange is ~(1–50) x 10^{-16} cm^2 in this energy range. Rather large deviations in cross-section values have been reported in some cases. In such cases, we use the lowest quantities, resulting in an underestimation of the LENA production. We consider only the charge exchange reactions that produce LENAs directly. For example, the reaction $O^{++} + S \rightarrow O^* + S^{++}$ is considered between doubly

charged ions (for example O^{++}) and neutrals (e.g. S). There are of course the reaction of single electron transfer, namely, $O^{++} + S \rightarrow O^{+} + S^{+}$. However, since this reaction does not produce LENAs directly, we should not consider it.

To simplify the calculation, we calculated the total cross section as defined below. First, we take the average of cross section for each parent ion species, weighted by the fraction of neutral composition. This is the "convolved cross section" in Table 1. This convolved cross section is the single value but equivalent to the cross section of a parent ion for charge exchange process through the multiple-species Io neutral torus. Here, the average relative composition of S and O near the neutral torus is 1:4 (e.g., Johnson and Strobel, 1982). The H population is assumed to be 10% of the total assuming stoichiometry. We neglect the molecular contributions to the cross-section calculations, primarily because we could not find good reference data to constrain the fraction and the charge exchange cross sections. Then, we again take the weighted average to obtain the total cross section for each LENA species, considering the parent ion's charge state. This is the cross section for charge exchange production for specific LENA species from different charge-state parent ions. The total calculated cross sections are 12, 19, and 9 x 10^{-16} cm^2 for H, O, and S, respectively (Table 1).

After calculating the LENA flux, we further evaluated if a conventional LENA sensor can measure the Io torus image. As a reference instrument used in this paper to calculate the LENA count rate to evaluate the measurement feasibility, we consider the current design of the JNA instrument (hereafter referred to as the JNA-prototype) prepared for the JUICE spacecraft. The JNA-prototype has similar capabilities to the MPPE/ENA sensor and Chandrayaan-1/CENA sensor (Kazama et al., 2006; Barabash et al., 2009). See Table 2 for a summary of the specifications of the JNA-prototype.

3. Model Results

3.1 Io-torus LENA flux

316 Figure 3 presents an image of simulated differential flux of the LENAs
317 emitted from the Io tori. The oxygen and sulfur LENA images for the energy of
318 210 eV and 420 eV (both for ~50 km/s) is displayed as examples. The observer
319 is placed at the planned location of the JUICE spacecraft during its so-called
320 high-latitude imaging period (Grasset et al., 2013). During this period, the
321 spacecraft will have a slight inclination with respect to the equatorial plane. We
322 show here the case when the spacecraft was located at 23.3 Rj at the latitude of
323 6.5˚ north from the Jovian equatorial plane.
324 The peak flux can reach 10^5 /cm^2 s eV sr in this case. The shape of the
325 LENA image is similar to a slice of the Io plasma torus. The image exhibits a
326 very narrow angular distribution. One can see a shift in the peak signal toward
327 Jupiter by ~10˚. This shift is caused by the spacecraft velocity effect (aberration).
328 The simulated image clearly illustrates that the contribution of the spacecraft
329 motion cannot be neglected. The spacecraft is typically moving at 10 km/s, and
330 thus, the aberration effect is, at maximum, ~10˚ for 50 km/s LENAs when the
331 ENA flow direction and the spacecraft velocity vector is perpendicular. When
332 they are parallel, this effect can be seen as a change in the observed ENA
333 velocity. The spacecraft velocity effect can be corrected by subtracting the
334 velocity of the spacecraft from the image in the actual data analysis (Appendix
335 A). Figure 3 also displays a strong signal from the "left" side of Jupiter in the
336 figure, where the north of Jupiter is drawn to be up. On this side, the Io tori
337 particles move toward the observer so that the generated ENAs fly to the
338 spacecraft. Although the corotation plasma undergoes charge exchange when
339 Io is located on the other side ("right" side in Figure 3) of Jupiter, the generated
340 LENAs will travel away from the spacecraft. Therefore, the instantaneous image
341 has a strong asymmetry. In the followings, we refer to the "left" side (strong
342 LENA flux) as toward side and the other as away side. The degree of toward-
343 away asymmetry depends on the temperature of the corotating plasma. More
344 asymmetry is expected for cooler plasma.
345 Figure 4 presents a series of LENA images taken along the planned orbit of
346 the JUICE spacecraft. Oxygen ENA images with the energy of 210 eV, same
347 condition as Figure 3, are shown as examples. The corresponding locations of

348 the spacecraft are marked at the center of the figure. The LENAs from the Io tori
349 are always seen from the toward side of Jupiter regardless of the relative position
350 of the observer with respect to Jupiter and Io. The peak flux varies from 10^3 to
351 10^5 /cm^2 s sr eV. In contrast, the intensity clearly depends on the relative
352 position. We can detect a strong flux from the Io tori when the LENAs that are
353 generated from the side with the corotating plasma move toward the spacecraft
354 (equivalently, when Io is located on the toward side of Jupiter). The highest flux
355 is obtained at Jupiter-Io-Observer angle of ~165˚ in this case (18 UT on May 20,
356 2031). This time is ~8 hours after the Jupiter-Io-Observer angle is 90˚ (at 10 UT
357 on May 20, 2031), when the maximum flux would be expected from the naïve
358 prediction. This apparent discrepancy can be simply explained once we
359 consider the flight time of the LENAs. Even if the maximum flux is produced
360 when the Jupiter-Io-Observer angle is 90˚, the LENAs take a few hours to reach
361 to the spacecraft. For oxygen LENAs with a speed of ~50 km/s, traversing the
362 distance of over 15 Rj (~10^6 km) from Io to the spacecraft takes 2x10^4 s (~6 h).
363 As one might expect, the time lag depends on the velocity of the LENAs.
364 The time series of the LENA count rate to be observed by the JNA
365 instrument (Table 2) at the JUICE location is shown in Figure 5. The spacecraft is
366 assumed to point toward Jupiter, and the right edge of the aperture is aligned
367 with Jupiter (gray dotted rectangle in Figure 3). The count rates of three species
368 (H, O, and S) are calculated by integrating the simulated LENA flux over the
369 sensor pixel shown in Figure 3. The calculated peak count rate is 1-100 counts
370 per second for all species. The O flux is most prominent because O is the
371 dominant species in the plasma torus. The mass-dependent bulk energy of each
372 species corresponds to the corotation velocity. Note that the peak energy
373 appears to be higher than the corotational energy in Figure 4; this is mainly
374 because the count rate is proportional, provided the g-factor is constant over the
375 energy, to the energy flux, not the particle flux, so that the peak count rate shifts
376 toward the higher energy.
377 The spectrogram displays several characteristic features. First, there is a
378 clear ~10 h periodicity. This periodicity arises from the rotation of the Jupiter's
379 magnetosphere. The neutral torus moves up and down with respect to the

plasma-torus structure, and the number of charge-exchange reactions varies accordingly, peaking when the magnetic equator is in line with the Io neutral torus. Second, there is a ~50 h periodicity. This periodicity is associated with the rotation of Io (and the resulting Io neutral torus) around Jupiter with a period of ~42.5 h. Precisely speaking, this periodic feature is the synodic period of Io and the spacecraft. We can also observe the dispersion-like signatures because of the flight time of the LENAs from the torus to the spacecraft, which depends on their velocity. A lower LENA energy will cause the LENA to take longer to reach the spacecraft. The time scale of the dispersion is several hours.

3.2 Loss of LENAs

After being generated near the Io tori, some LENAs may be lost before arriving at the spacecraft. Thus, we must evaluate the importance of the loss processes. Here, three loss mechanisms are considered: electron impact ionization, charge exchange, and photoionization.

The probability of electron impact ionization p_{ei} is estimated as follows:

$$p_{ei} = \int_0^\infty n_e(l)\sigma_{ei}(E)dl \sim \langle n_e \rangle \sigma_{ei} L$$

where n_e and $<n_e>$ are the electron density and its average along the trajectory, respectively; l is the distance along the trajectory; σ_{ei} is the electron impact ionization cross section, which is a function of the impact energy; and L is the typical scale length.

To determine the upper limit, let us consider the maximum cross section $\sigma_{ei} = 1.5 \times 10^{-16}$ cm^2 (for ~100 eV electrons; Kim and Desclaux, 2002) and the maximum electron density ~2000 cm^{-3} (near Io; Kivelson et al., 2004) over the traveling length of L = 15 Rj (~10^{11} cm). The resultant calculated probability of electron impact ionization is $p_{ei}=<n_e>\cdot \sigma_{ei} \cdot L=3 \times 10^{-2}$. This value includes a large margin for error, and in reality, the loss probability must be considerably smaller. The electron temperature is ~10 eV at Io's orbit (Kivelson et al., 2004), which is smaller than the oxygen ionization potential. In this case, the cross section for ionization is negligible. The electron temperature reaches a few 100 eV near Europa or Ganymede, while in these regions, the electron density is one to two

orders of magnitude smaller than the assumed density. The high-energy tail (including radiation-belt energy) of the electrons contributes to the ionization, but the cross section is again much smaller (e.g. Itikawa and Ichimura, 1990).

The generated LENAs can also experience charge exchange once again with other ions, thereby becoming re-ionized. The generated ions begin corotating around Jupiter, and the generated neutral atoms should be considered as ENAs, but their velocities become consistent with the local corotational speed. A similar calculation can be performed as for electron impact ionization, and the probability of charge exchange is

$$p_{\mathrm{cx}} = \int_0^\infty n(l)\sigma_{\mathrm{cx}} dl \sim \langle n \rangle \sigma_{\mathrm{cx}} L$$

The density, $<n>$, is the density of the plasma and takes a maximum value of 2000 cm^{-3}; σ_{cx} can reach as high as 10^{-15} cm^2. If the distance L is taken along the whole travelling length of 15 Rj (~10^{11} cm), the loss fraction calculated using these values is 0.2. Again, the obtained value is an upper limit with a large margin for error, particularly because of the plasma and neutral densities quickly decreases from the Io orbit. Plasma density drops by one order beyond 2 Rj (Figure 2b). The neutral density drops much quicker (Figure 1). Therefore, the loss fraction should be much lower in reality, more than by one order (<<0.02).

Photoionization is another potential loss process. The ionization potentials for the relevant species are ~10 V (10.4 V for S and 13.6 V for O and H), and thus, the impinging photons should have energies of more than 10 eV (wave length <100 nm; V-UV, E-UV and shorter). The only possible source of such short-wavelength photons is the Sun. At the typical solar irradiance, the power in this wavelength range is rather constant at 10^{-4} W m^{-2} nm^{-1} at 1 AU (e.g., Schmidtke et al., 2006). Thus, the total photon flux can then be estimated to be ~$3x10^8$ cm^{-2} s^{-1}, and at the Jupiter orbit (~5.9 AU), it is reduced to ~10^7 cm^{-2} s^{-1} integrated over wavelengths of <100 nm. The cross section of the photoionization reaches a maximum of ~$2x10^{-17}$ cm^2 at 65–70 nm for oxygen atoms, according to the EUVAC model (Richards et al., 1994). To obtain an upper limit, we simply take the peak value over the entire wavelength range,

443 which yields a loss rate of ~2×10^{-10} s^{-1}, and thus, the minimum LENA lifetime is
444 estimated to be 5×10^{9} s. This lifetime is sufficiently long compared with the
445 flight time of LENAs (10^{4}–10^{5} s) that we can neglect the loss caused by
446 photoionization.
447 In conclusion, ENA loss between the Io tori and the observer is not very
448 large, and thus is not critical for Io-tori LENA imaging. Indeed, because the
449 energy range of interest in this work is rather restricted, the energy dependence
450 of all loss mechanisms is weak so the shape of the energy spectrum is conserved.
451 Thus, losses of LENAs do not significantly impact the feasibility of LENA
452 imaging and associated scientific achievements.

453 **3.3 Sensor capabilities**

454 The expected differential flux is typically ~10^{3}–10^{5} cm^{-2} s^{-1} sr^{-1} eV^{-1}
455 (Figures 3 and 4) at the Ganymede distance. This flux corresponds to ~1–100
456 counts per second by considering the JNA-prototype performance at the JUICE
457 planned orbit (Figure 5). However, one difficulty of collecting instantaneous
458 observations of Io torus ENA from the Ganymede distance is that Io LENAs have
459 a narrow angular beam-like structure with a full width half maximum of <5°,
460 which is rather small in comparison with the JNA-prototype angular resolution
461 of ~30x5°. Thus, fine structures may be hidden in one angular pixel. Better
462 angular resolution is required to resolve these fine structures. Although the peak
463 count rate is enough in the detectable level, a longer integration time may be
464 beneficial for investigating the energy spectrum or the spatial distributions. For
465 example, a change in the global morphology of LENA specta, such as the
466 dispersion relations seen in Figure 5, can be identified even when integrating
467 over several to tens of minutes. Let us suppose here a 10-min integration (during
468 which the spatial configuration would not change significantly) with 8 energy
469 steps, then ~75 s integration is possible for each energy step, and the
470 corresponding number of counts will be increased to 75–7500 counts. Indeed, a
471 longer time integration will also aid in decreasing the telemetry and in reducing
472 the ambiguity of background counts that originate from the intense Jovian
473 radiation environment.

4. Scientific objectives

In this section, we discuss what information can be obtained from LENA measurements of the Io tori and what scientific objectives we can address using these data. Table 3 summarizes the quantities that LENA data can (and cannot) provide. Detailed explanations and justifications are discussed in the following.

4.1 Io-tori characterization

LENA data can provide physical quantities that describe the plasma torus. The shape of the energy spectrum of the LENAs and their chemical (mass) composition can be obtained. The energy spectra directly reflect those of the Io torus plasma, thereby, providing information that is critical to understanding the characteristics and dynamics of the plasma in the plasma torus. The velocity of the plasma in the torus and its temperature can also be calculated using the LENA measurement. The absolute densities of the neutral and plasma tori cannot be easily deconvolved from the LENA dataset alone because the LENA data provide only a line-of-sight integral of a convolution of both densities.

The mass information reflects the chemical composition in the plasma torus. The mass composition is strongly influenced by generation and loss mechanisms (e.g. Frank and Paterson, 2001; Delamere et al., 2004; Hansen et al., 2005; Steffl et al., 2006). For example, if the O^+/S^+ ratio is two, one may infer, under the stoichiometric assumption, that the Io plasma torus originates from volcanic Io materials (SO_2) and that the loss mechanism does not depend on species. Deriving the mass fraction of H^+ will aid in understanding the dynamics of protons in the Jovian magnetosphere. Proton distribution in the Io torus is not a well constrained information (e.g. Thomas et al. 2004). Although the proton fraction has been assumed 10%, there are several measurements showing much smaller fraction than 10% (e.g. Wang et al., 1998a, b; Zarka et al., 2001). The discrepancies indicate strong spatial or temporal variations. LENA imaging can reveal proton fraction and its spatial distribution instantaneously.

503 The charge state of ions in the plasma torus, e.g., S^+ and S^{++}, might be
504 derived from the different shapes of the energy spectra. Because of the M/q
505 difference between different charge states, different charge-state ions of the
506 same species can have different energy spectra (e.g., temperatures). For example,
507 S^{++} (M/q = 16) is expected to have a temperature similar to O^+ (M/q = 16) but
508 different from S^+ (M/q = 32), if one attributes the ion temperatures in the plasma
509 torus to the pickup process. It is also believed that the Io plasma torus is not in
510 chemical equilibrium (e.g., Thomas et al., 2004), implying that there is no
511 reason that S^+ and S^{++} should have the same spectral shape. The separation of
512 charge states using the LENA velocity distribution functions may be a realistic
513 goal.
514 Whereas the LENA energy spectra and LENA mass spectra reflect the
515 plasma-torus characteristics well, the neutral-torus characteristics are more
516 difficult to obtain. In theory, the velocity of the neutrals in the torus and the
517 mass composition are convoluted in the cross section. However, to extract this
518 information from the actual data is quite difficult. There is an uncertainty in the
519 velocity dependence of the cross section. The charge-exchange cross sections
520 associated with S are particularly difficult to obtain in laboratory measurements,
521 as S tends to react chemically with ambient gas and instrumentation. Thus, we
522 must refer to theoretical calculations (e.g. Johnson and Strobel, 1982). Other
523 complimented observations (Section 5.2) or modelling effort to restrict the LENA
524 data interpretation (Section 5.2) would be more realistic way of investigation.

525 **4.2 Short-term variations**

526 Short-term temporal variations (or, in particular, abrupt variations) in the
527 plasma and neutral tori, if they occur, can result in corresponding variations in
528 the LENA flux. From continuous time series of LENA energy and mass spectra,
529 one can identify which of the tori is responsible for the LENA variation. This
530 separation can be achieved because of the different responses of the LENA flux
531 to the changes in the plasma and neutral tori. When the density of the neutral
532 torus increases abruptly for some reason, the LENA flux increases regardless of
533 energy and mass; more precisely speaking, the change would be proportional

534 the cross sections to the relative, but it can be distinguished. In contrast, there is
535 a high likelihood that a temporal variation in the plasma torus would induce
536 modifications only at specific energies and/or masses. For example, in the case
537 of sporadic injection of plasma into the plasma torus, the LENA image would be
538 affected only at the corresponding energy and/or mass of the injection.
539 Another possible phenomenon for investigation is the hypothetical O and
540 S streams. Na is known to exhibit a short temporal scale (<10 hours) and
541 relatively small spatial scale (a few Io radii) stream (e.g., Schneider et al., 1991;
542 Wilson et al., 2002; Thomas et al., 2004; Schneider and Bagenal 2007).
543 Although the existence of similar streams for O and S is thought to be less
544 plausible because of the different characteristics (timescales and chemical
545 reactions) of Na, O, and S, LENA imaging may provide information to place
546 limit on the existence of fast O and S stream in the near Io environment.

547 **4.3 Long-term variations**

548 From Galileo observations, the plasma-torus density is known to vary
549 significantly over time. Frank and Paterson (2001) claimed that the density of
550 the Io plasma torus during the 1995 flyby was three to four times higher than
551 during the other flybys in 1999 and 2000. One of the hypothetical sources of
552 enhancement of the Io tori is variable volcanic activity. Indeed, the UV
553 measurement performed by Cassini indicates a long-term (week to month)
554 change in the tori, which may be attributed to volcanic activity (Schneider and
555 Bagenal, 2007). Ground-based observations indicate systematic long-term
556 correlations between the volcanic activities and the emission of IR (Nozawa et
557 al., 2004; Yoneda et al., 2010).
558 If volcanic activities increase, the neutral-torus density initially increases.
559 After a period of time (the ionization time scale depends on the mechanisms,
560 being typically a few hours; e.g., Smyth and Combi, 1988; Schneider and
561 Bagenal., 2007), the higher-density neutrals become ionized to form a denser
562 plasma torus. The higher density plasma torus may retain more than 10s of days
563 (e.g. Schneider and Bagenal, 2007). We can monitor the evolution of the Io tori
564 by tracking these temporal changes; first ENA flux increases almost independent

565 of the species and energies because of the increase of neutral component,
566 followed by species-by-species energy dependent increase due to the increase
567 of the plasma composition, depending on the generation and loss mechanisms.

568 **4.4 Transport**

569 ENAs are considered to be one of the transport mechanisms of materials
570 from the Io orbit outward. Because of Io's volcanic activity ~10^{28} particles are
571 introduced into the neutral torus per second, and (1-2)x10^{26} ions are transported
572 out of the Jovian system per second via the charge-exchanged ENAs in the high-
573 energy domain of the Cassini/INCA sensor (Krimigis et al., 2002). These authors
574 also inferred that the total escape flux, including lower energies, is 10^{27}/s, which
575 is 10% of the generated flux. The direct measurement of the LENAs will provide
576 a more precise estimate of the loss rate from the torus via the charge exchange.
577 Figure 6 shows the LENA distribution seen on the global scale of the Jovian
578 magnetosphere. Each dot corresponds to a LENA, which are emitted from Io tori
579 with the velocity of the corotation and a thermal spread of 5.5 km/s (T~70 eV
580 for O is assumed). The global LENA distribution forms a spiral shape, although
581 each LENA is traveling almost radially. This spiral shape is conceptually similar
582 to the Parker spiral of the solar wind magnetic field or water ejected from a
583 rotating sprinkler. To produce this plot, we did not consider the Jovian magnetic
584 field tilt for simplicity. Inclusion of the tilt will embed a ~10 hour modulation
585 (corresponding to ~85˚ in the azimuthal direction).
586 The transfer from Io is not axisymmetric inside the Jovian magnetosphere.
587 If one is located at a certain point, the LENA flux from the Io torus is measured
588 as an intermittent flow. In contrast, the thermal spread of the Io plasma and
589 distribution of the generation point (although it is close to Io position) will
590 dissipate the shape of the spatial distribution in the very far tail (>~150 *Rj* with
591 the parameters used in this calculation). This image can be complemented by
592 the "neutral nebula" concept formulated by Krimigis et al. (2002), in which they
593 suggested a disk-like confinement of LENAs in the Jovian equatorial plane
594 generated by Io's (or other moons') tori. However, the view provided in Figure 6
595 indicates a spiral structure inside the nebula.

4.5 Lag of the plasma corotation

Based on Voyager 1 plasma sensor data, McNutt et al. (1979) reported that the Jovian magnetosphere exhibits a slightly slower than "perfectly" rigid corotational flow. This velocity lag has been identified even at Io's distance. The in situ plasma measurements collected by Galileo indicated that the lag is ~2–10 km/s, with an average lag of 2–3 km/s (Frank and Paterson, 2001). Higher velocities than the corotational velocity have never been observed. Hill (1980) suggested that the lag is the effect of mass loading. Another suggested mechanism is the hypothetical latitudinal differential rotation of the Jovian magnetosphere (Dessler 1985). Long-term observations permitting the characterization of the velocity of the plasma torus can restrict the possible slow-down mechanisms of the plasma torus in the vicinity of Io. If we can point the FOV of JNA perpendicular to the magnetic equatorial plane (perpendicular to the pixel shown in Figure 3), the collected LENA data along the FoV will provide the latitudinal difference in the torus velocity. This operation will test the differential-rotation hypothesis. By investigating the correlations between the torus densities and the velocity lag determined from LENA measurements, one may also constrain the momentum transfers between the plasma and neutral tori, which directly contribute to the mass loading.

The typical velocity lag is 2–3 km/s, which corresponds to ~3–4% of the corotational velocity (and to ~5-8 % of the energy). Distinguishing an energy difference of <10% from JNA data may not be a straightforward analysis, but it should still be possible if one employs proper analysis methods. For example, as in Futaana et al. (2013), it is possible to clearly distinguish the LENA flux for parametric temperatures of ~85 eV from that for 75 eV (a ~10% difference in energy). When the velocity lag is as large as 5–10 km/s (~7–13% of the corotational flow), the energy difference becomes ~15–25%, and the possibility of the discrimination becomes more promising.

5. Operation, Collaboration, and Data analysis

5.1 Challenges

Although a sufficient count rate of LENAs from the Io tori is expected, operating the LENA instrument during the real mission and analyzing the obtained data pose a considerable challenge. The limited field of view (FOV) is the most problematic issue. The FOV of the existing LENA sensors is a single-pixel camera (McComas et al., 2009) or a fan-shaped 1-D aperture (Barabash et al., 2009), and thus, the angular acceptance is very small. When this small acceptance is combined with the relatively small angular spread of the Io-torus LENA image, a small shift in the aperture results in the loss of the LENA signal peak. Although we may know the predicted attitude of the spacecraft beforehand in the practical operation, pointing toward the Io torus is not a simple task. The spacecraft velocity (ram velocity) is not negligible for Io-torus LENA imaging (Figures 3 and 4), and the optimal compensating angle depends on the energy of LENAs. Thus, there is no unique optimal solution for spacecraft pointing that captures the maximum fluxes for all energies. A rather good argument here is that the data analysis after data reception is simpler because all information necessary to correct the aberration effect is known.

The second problem is the LENA flight time. The typical measurement of the Io torus by the JUICE spacecraft will be performed at the Ganymede orbit (~15 Rj) or farther. For the LENA with a velocity of 74 km/s, the flight time is ~1.4×10^4 s. Because Io rotates around Jupiter in ~42.5 h, Io moves more than 30° in the time it takes for the LENAs to reach the instrument. For the instrumental operation, we should refer not to the Io's position at the operating time but the position several hours before depending on the LENA energy. As shown in Figure 4, we can clearly see a peak emission a few hours after the apparent optimal condition.

Third, the gravitational force exerted by Jupiter affects the LENA trajectories and causes them to become to ballistic trajectories. The degree of bending depends on the velocity, but the low-velocity LENAs are most strongly affected. The gravitation force is a well-known parameter, and its influence is smaller than that of the flight time discussed above; however, the gravity force must be properly considered for precise analysis of the obtained data.

Fourth, the charge-exchange cross sections are still not well constrained. They also depend on the relative velocities between the plasma and neutral particles in the tori. However, the dependency is not very strong within the LENA energy range. For example, for the O^+–O interaction, the variation with energy is approximately a factor of two to three between 40 eV and 10 keV (Lindsay and Stebbings, 2005). Nevertheless, when one calculates the physical quantities of the tori (e.g., the density, composition, and other quantities) from the obtained data, the uncertainty of the cross sections directly impacts the uncertainties of those quantities.

5.2 Synergy with Other Measurements

HENAs are also expected from high-energy particles in the plasma torus. JNA will be accompanied by the Jovian Energetic Neutrals and Ions (JENI) sensor, which is also included as a part of the PEP suite to detect HENAs. Their energy range is planned to cover 0.5–300 keV. HENAs will be detected even when fewer LENAs are detected (when Io is on the away side) because of the high thermal velocity of the original ions. HENAs provide information regarding characteristics of the Io torus plasma and Io's radiation environment, and moreover, they may preserve information concerning acceleration mechanisms. Thus, the combination of LENA and HENA time-series data will permit the investigation of the evolution of the acceleration of plasma in the plasma torus. In addition, JENI is capable of 2-D imaging. The simultaneous JENI imaging will extend the observable velocity and mass space of ENAs.

Another related science target to be investigated via the synergy between LENA and HENA data is the trans-Europa gas tori (Mauk et al., 2003). Based on a HENA (50–80 keV) image obtained using the Cassini/INCA instrument, the existence of Europa gas tori (composed of H and O) has been suggested, although this instrument has found no evidence of distinct Io-tori related HENAs. The corotational velocity at the Europa orbit is ~150 km/s, and thus, the core component (H and O) of ENAs generated in the Europa-tori also falls into the LENA energy range. Sulfur may reach ~4 keV, which is almost the upper limit of the JNA sensor. A LENA measurement will provide complimentary evidence of

688 the existence of trans-Europa gas tori. Distinguishing between the Io and Europa
689 tori from LENA data alone will not be simple because the JNA-prototype has a
690 rather coarse angular resolution (Table 2). However, it will still be possible to
691 distinguish between the Io and Europa tori using the energy spectra and their
692 periodic features, the dispersion signatures and the mass spectra. The energy
693 spectrum of LENAs from Io should have a peak at ~74 km/s, whereas the LENAs
694 from Europa should have a peak at ~150 km/s, corresponding to their respective
695 corotation velocities. In addition, the periodicity of the ENA signals, as seen in
696 Figure 5, must differ according to the moons' rotation period.
697 LENA imaging can be compared with observations of UV emission to gain
698 further understanding of the Io tori. The UV and LENA measurements are both
699 imaging, so that the obtained data can be used complimentarily. A difference of
700 characteristics is the LENA line-of-sight (trjaectory) is twisted by the gravity of
701 Jupiter; therefore the different slice of of the information may be obtained. If the
702 neutral (plasma) density is derived via the UV spectroscopy, the plasma (neutral)
703 density can be derived using a LENA sensor, in principle. Another difference is
704 the emission signature. Since the photon is emitted isotropically, the obtained
705 image will be fundamentally different from the highly directional emission of
706 LENAs. For example, the Io-torus UV emission measured using the EUVE
707 satellite exhibits a dawn-dusk asymmetry, in which the dusk side is stronger,
708 and there is no apparent Io-phase dependence (Gladstone and Hall, 1998). In
709 contrast, the Voyager UV measurement did indicate an Io-phase dependence
710 (Sandel and Broadfoot, 1982). These features in the UV images differ from the
711 predicted LENA images, which exhibit a clear toward-away asymmetry in which
712 the toward side is stronger. Although the toward-dusk asymmetry of the Io tori is
713 essential to understanding the generation and loss mechanisms and the
714 dynamics of particles in the tori, placing constraints on the asymmetry using the
715 LENA dataset is a difficult task because the peak flux of the LENAs on the away
716 side will never reach the spacecraft (because of the strongly directional flow of
717 LENAs). This indicates that the LENA imaging have a information gap depending
718 on the Io position: Recurrence of the measurement is ~50 hour for LENAs, so
719 that any changes below the time scale in LENA signatures are hardly attributed

to either the change in the neutral or the plasma tori. UV imaging will help to fill the gap of this information. Indeed, variations in such time scales have been reported. Many authors (e.g. Sandel and Dessler, 1988; Brown 1995; Frank and Petersen, 2001; Nozawa et al., 2004; Steffl et al., 2006) argued that a typical variation in tori characteristic period could be modulated by the so-called System IV period (~10.2 hours). Cassin UV spectroscopy reported the enhancement of the torus emission power by 20% for about 20 hours (Steffl et al., 2004). Such phenomena in these time scales are difficult to investigate only from LENA imaging.

Synergy with state-of-the-art data-analysis algorithms should also be mentioned here. The JNA-prototype provides angular separation in only one direction of the angle, which will limit the intuitive understanding of the LENA signal. We may require the aid of numerical models and/or inversion techniques. Such inversion techniques have been applied beginning with the early ENA observations (e.g., Demajistre et al., 2004; Galli et al., 2008a; 2008d; Nakano et al., 2008). Similar techniques should be optimized for each scientific objective, implemented and validated for interpreting LENAs that originate from the Io tori, considering all the affecting parameters (spacecraft velocity, flight time, and gravity).

5.3 Impact on spacecraft and mission design

One benefit of LENAs compared with in situ measurements is that LENAs can enable the remote sensing of particles in the Io tori. Without actually entering to Io's orbit, we can investigate the near-Io neutral and plasma environment. A harsher will make the spacecraft and instrument designs more challenging. In addition, the background caused by radiation cannot be avoided, so one requires multiple-coincidence detection systems or longer time integrals to improve the signal-to-noise ratio for an in situ plasma sensor. These approaches typically lower the instrument sensitivity by a factor of 10–100.

6. Summary

We have calculated the flux and expected count rate of energetic neutral atoms in the low-energy domain (LENA) from the Io plasma and neutral tori. The expected total flux is 10^3–10^5 cm^{-2} s^{-1} sr^{-1} eV^{-1}, if one measures from the Ganymede orbit. The flux is comparable to or above the one-count-per-second level of the LENA sensor that has been designed for Jupiter exploration.

The time scale of the variation in the global morphology of the LENA flux is the rotation time of the Jupiter magnetosphere, which is ~10 h. A longer time scale of ~50 h, which corresponds to the synodic period of Io and the spacecraft, is also expected. Because of the flight time of LENAs, the LENA energy spectrum exhibits dispersion signatures, typically with a time scale of several hours. The angular spread is rather confined, and thus, the LENA sensor should be improved to achieve higher angular resolution for resolving fine structures.

In 2030, the Jupiter exploration mission JUICE will conduct the first Jovian LENA measurement using a LENA instrument, JNA. From LENA observations, we can derive the characteristic quantities such as the energy spectra, density, velocity, and the composition of plasma-torus particles. We can further investigate the temporal variations (both short- and long-term) of the tori, the transport of materials, and acceleration mechanisms.

Acknowledgments

The authors appreciate the development and provision of the cross-section database (http://physics.nist.gov/PhysRefData/Ionization/Xsection.html) operated by the National Institute of Standards and Technology (NIST).

Reference

Acuña, M. H., and N. Ness, The main magnetic field of Jupiter, *J. Geophys. Res.*, *81* (16), 2917–2922, doi:10.1029/JA081i016p02917, 1976.

Bagenal, F., and J. D. Sullivan, Direct plasma measurements in the Io torus and inner magnetosphere of Jupiter, *J. Geophys. Res.*, *86* (A10), 8447–8466, doi:10.1029/JA086iA10p08447, 1981.

Bagenal, F., Empirical model of the Io plasma torus: Voyager measurements, *J. Geophys. Res., 99*, 11,043–11,062, doi:10.1029/93JA02908, 1994.

779 Bagenal, F., The ionization source near Io from Galileo wake data, *Geophys.*
780 *Res. Lett., 24* (17), 2111–2114, doi:10.1029/97GL02052, 1997a.
781 Bagenal, F., F. J. Crary, A. I. F. Stewart, N. M. Schneider, D. A. Gurnett, W. S.
782 Kurth, L. A. Frank, and W. R. Paterson, Galileo measurements of plasma
783 density in the Io torus, *Geophys. Res. Lett., 24*(17), 2119–2122,
784 doi:10.1029/97GL01254, 1997b.
785 Bagenal, F., and P. A. Delamere, Flow of mass and energy in the
786 magnetospheres of Jupiter and Saturn, *J. Geophys. Res., 116*, A05209,
787 doi:10.1029/2010JA016294, 2011.
788 Barabash, S., A. V. Lukyanov, P. C. Brandt, and R. Lundin, Energetic neutral
789 atom imaging of Mercury's magnetosphere 3: Simulated images and
790 insrtument requirements, *Planet. Space Sci., 49*, 1685–1692,
791 2001.Barabash, S., et al., The Analyzer of Space Plasmas and Energetic
792 Atoms (ASPERA-3) for the Mars Express mission, *Space Sci. Rev., 126*
793 (1), 113–164, 2006.
794 Barabash, S., et al., The Analyser of Space Plasmas and Energetic Atoms
795 (ASPERA-4) for the Venus Express mission, *Planet. Space Sci., 55* (12),
796 1772–1792, doi:10.1016/j.pss.2007.01.014, 2007.
797 Barabash, S., et al., Investigation of the solar wind-Moon interaction on board
798 Chandrayaan-1 mission with the SARA experiment, *Current Science*, *96*
799 (4), 526–532, 2009.
800 Brandt, P. C., D. G. Mitchell, E. C. Roelof, S. M. Krimigis, C. P. Paranicas, B. H.
801 Mauk, J. Saur, and R. DeMajistre, ENA imaging: seeing the invisible,
802 *Johns Hopkins APL technical digest*, *26* (2), 143, 2005.
803 Brown, R. A., Optical line emission from Io, in *Exploration of the Planetary*
804 *System*, edited by R. A. Brown, pp. 527–531, Reidel, 1974.
805 Brown, M. E., Periodicities in the Io plasma torus, J. Geophys. Res., 100,
806 21,683–21,695, 1995.
807 Burch, J. L., IMAGE mission overview, *Space Sci. Rev., 91* (1-2), 1–14,
808 doi:10.1023/A:1005245323115, 2000.
809 Burch, J., The first two years of Image, *Space Sci. Rev., 109*, 1–24,
810 doi:10.1023/B:SPAC.0000007510.32068.68, 2003.

811 Cheng, A. F., Energetic neutral particles from Jupiter and Saturn, *J. Geophys.*
812 *Res.*, *91* (A4), 4524–4530, doi:10.1029/JA091iA04p04524, 1986.
813 Connerney, J. E. P., M. H. Acuña, N. F. Ness, and T. Satoh, New models of
814 Jupiter's magnetic field constrained by the Io flux tube footprint, *J.*
815 *Geophys. Res.*, *103* (A6), 11,929–11,939, doi:10.1029/97JA03726,
816 1998.
817 Delamere, P. A., A. Steffl, and F. Bagenal, Modeling temporal variability of
818 plasma conditions in the Io torus during the Cassini era, *J. Geophys.*
819 *Res., 109*, A10216, doi: 10.1029/2003JA010354, 2004.
820 DeMajistre, R., E. C. Roelof, P. C. Brandt, and D. G. Mitchell, Retrieval of global
821 magnetospheric ion distributions from high-energy neutral atom
822 measurements made by the IMAGE/HENA instrument, *J. Geophys. Res.*,
823 *109* (A04214), doi:10.1029/2003JA010322, 2004.
824 Dessler, A. J. (Ed.), *Physics of the Jovian Magnetosphere*, Cambridge University
825 Press, 1983.
826 Dessler, A. J., Differential rotation of the magnetic fields of gaseous planets,
827 *Geophys. Res. Lett.*, *12* (5), 299–302, doi:10.1029/GL012i005p00299,
828 1985.
829 Divine, N., and H. B. Garrett, Charged particle distributions in jupiter's
830 magnetosphere, *J. Geophys. Res.*, *88* (A9), 6889–6903, 1983.
831 Dougherty, M. K., A. Balogh, D. J. Southwood, and E. J. Smith, Ulysses
832 assessment of the Jovian planetary field, *J. Geophys. Res.*, *101* (A11),
833 24,929–24,941, doi:10.1029/96JA02385, 1996.
834 Frank, L. A., and W. R. Paterson, Survey of thermal ions in the Io plasma torus
835 with the Galileo spacecraft, *J. Geophys. Res.*, *106* (A4), 6131–6149,
836 doi:10.1029/2000JA000159, 2001.
837 Futaana, Y., S. Barabash, M. Holmström, and A. Bhardwaj, Low energy neutral
838 atoms imaging of the Moon, *Planet. Space Sci.*, *54* (2), 132–143,
839 doi:10.1016/j.pss.2005.10.010, 2006.
840 Futaana, Y., J.-Y. Chaufray, H. Smith, P. Garnier, H. Lichtenegger, M. Delva, H.
841 Gröller, and A. Mura, Exospheres and energetic neutral atoms of Mars,

842 Venus and Titan, *Space Sci. Rev.*, *162*, 213–266, doi:10.1007/s11214-
843 011-9834-4, 2011.
844 Futaana, Y., et al., Empirical energy spectra of neutralized solar wind protons
845 from the lunar regolith, *J. Geophys. Res.*, *117* (E5), E05005,
846 doi:10.1029/2011JE004019, 2012.
847 Futaana, Y., S. Barabash, M. Wieser, C. Lue, P. Wurz, A. Vorburger, A.
848 Bhardwaj, and K. Asamura, Remote energetic neutral atom imaging of
849 electric potential over a lunar magnetic anomaly, *Geophys. Res. Lett.*,
850 *40*, 262–266, doi:10.1002/grl.50135, 2013.
851 Galli, A., et al., Tailward flow of energetic neutral atoms observed at Venus, *J.*
852 *Geophys. Res.*, *113*, E00B15, doi:10.1029/2008JE003096, 2008a.
853 Galli, A., et al., Tailward flow of energetic neutral atoms observed at Mars, *J.*
854 *Geophys. Res.*, *113* (E12), E12012, doi:10.1029/2008JE003139, 2008b.
855 Gladstone, G. R., and D. T. Hall, Recent results from EUVE observations of the
856 Io plasma torus and Jupiter, *J. Geophys. Res.*, *103* (E9), 19,927–19,933,
857 doi:10.1029/98JE00823, 1998.
858 Goldstein, J., and D. J. McComas, Five years of stereo magnetospheric imaging
859 by TWINS, *Space Sci. Rev.*, doi:10.1007/s11214-013-0012-8, 2013.
860 Grande, M., Investigation of magnetospheric interactions with the hermean
861 surface, *Adv. Space Res., 19*(10), 1609–1614, 1997.
862 Grasset, O., et al., JUpiter ICy moons Explorer (JUICE): An ESA mission to orbit
863 Ganymede and to characterise the Jupiter system, *Planet. Space Sci.*, *78*
864 (0), 1–21, doi:10.1016/j.pss.2012.12.002, 2013.
865 Gruntman, M., Energetic neutral atom imaging of space plasmas, *Rev. Sci.*
866 *Instrum., 68*, 3617, 1997.
867 Hansen, C. J., D. E. Shemansky, and A. R. Hendrix, Cassini UVIS observations
868 of europa's oxygen atmosphere and torus, *Icarus, 176* (2), 305–315,
869 doi:http://dx.doi.org/10.1016/j.icarus.2005.02.007, 2005.Herbert, F., G.
870 R. Gladstone, and G. E. Ballester, Extreme ultraviolet explorer spectra of
871 the Io plasma torus: Improved spectral resolution and new results, *J.*
872 *Geophys. Res., 106*(A11), 26,293–26,309, doi:10.1029/2000JA002501,
873 2001.

874 Herbert, F., N. M. Schneider, A. R. Hendrix, and F. Bagenal, Hubble space
875 telescope observations of sulfur ions in the io plasma torus: New
876 constraints on the plasma distribution, *J. Geophys. Res., 108*(A5), 1167,
877 doi:10.1029/2002JA009510, 2003.
878 Hill, T. W., A. J. Dessler, and F. C. Michel, Configuration of the jovian
879 magnetosphere, *Geophys. Res. Lett., 1*(1), 3–6,
880 doi:10.1029/GL001i001p00003, 1974.
881 Hill, T. W., and F. C. Michel, Heavy ions from the Galilean satellites and the
882 centrifugal distortion of the Jovian magnetosphere, J. Geophys. Res., 81,
883 4561, doi:10.1029/JA081i025p04561, 1976.
884 Hill, T. W., Corotation lag in Jupiter's magnetosphere: Comparison of
885 observation and theory, *Science*, *207* (4428), 301–302,
886 doi:10.1126/science.207.4428.301, 1980.
887 Itikawa, Y., and A. Ichimura, Cross sections for collisions of electrons and
888 photons with atomic oxygen, *J. Phys. Chem. Ref. Data*, *19* (3), 637–651,
889 doi:10.1063/1.555857, 1990.
890 Johnson, R. E., and D. F. Strobel, Charge exchange in the Io torus and exosphere,
891 *J. Geophys. Res.*, *87* (A12), 10,385–10,393,
892 doi:10.1029/JA087iA12p10385, 1982.
893 Kazama, Y., S. Barabash, A. Bhardwaj, K. Asamura, Y. Futaana, M. Holmström,
894 R. Lundin, R. Sridharan, and P. Wurz, Energetic neutral atom imaging
895 mass spectroscopy of the moon and mercury environments, *Advances*
896 *in Space Research*, *37* (1), 38–44, doi:doi: 10.1016/j.asr.2005.05.047,
897 2006.
898 Kim, Y. K., and J. P. Desclaux, Ionization of carbon, nitrogen, and oxygen by
899 electron impact, *Phys. Rev. A*, *66*, 012708,
900 doi:10.1103/PhysRevA.66.012708, 2002.
901 Kirsch, E., S. M. Krimigis, J. W. Kohl, and E. P. Keath, Upper limits for X-Ray
902 and energetic neutral particle emission from Jupiter: Voyager-1 results,
903 *Geophys. Res. Lett.*, *8* (2), 169–172, doi:10.1029/GL008i002p00169,
904 1981.

905 Kivelson, M. G., F. Bagenal, W. S. Kurth, F. M. Neubauer, C. Paranicas, and J.
906 Saur, Magnetospheric interactions with satellites, in *Jupiter: The Planet,*
907 *Satellites and Magnetosphere*, chap. 21, pp. 513–536, Cambridge
908 University Press, 2004.
909 Krimigis, S. M., T. P. Armstrong, W. I. Axford, C. O. Bostrom, C. Y. Fan, G.
910 Gloeckler, and L. J. Lanzerotti, The low energy charged particle (LECP)
911 experiment on the Voyager spacecraft, *Space Sci. Rev.*, *21*, 329–354,
912 doi:10.1007/BF00211545, 1977.
913 Krimigis, S. M., et al., A nebula of gases from Io surrounding Jupiter., *Nature*,
914 *415* (6875), 994–996, doi:10.1038/415994a, 2002.
915 Kupo, I., Y. Mekler, and A. Eviatar, Detection of ionized sulfur in the Jovian
916 magnetosphere, *ApJ, 205*, L51–L53, doi:10.1086/182088, 1976.
917 Lindsay, B. G., and R. F. Stebbings, Charge transfer cross sections for energetic
918 neutral atom data analysis, *J. Geophys. Res.*, *110* (A12),
919 doi:10.1029/2005JA011298, 2005.
920 Massetti, S., S. Orsini, A. Milillo, A. Mura, E. De Angelis, H. Lammer, and P.
921 Wurz, Mapping of the cusp plasma precipitation on the surface of
922 mercury, *Icarus, 166*(2), 229–237, 2003.
923 Mauk, B. H., D. G. Mitchell, S. M. Krimigis, E. C. Roelof, and C. P. Paranicas,
924 Energetic neutral atoms from a trans-Europa gas torus at Jupiter, *Nature*,
925 *421* (6926), 920–922, doi:10.1038/nature01431, 2003.
926 McComas, D., et al., IBEX—Interstellar Boundary Explorer, *Space Sci. Rev.*, *146*
927 (1), 11–33, doi:10.1007/s11214-009-9499-4, 2009.
928 McGrath, M. A., and R. E. Johnson, Charge exchange cross sections for the Io
929 plasma torus, *J. Geophys. Res.*, *94* (A3), 2677–2683,
930 doi:10.1029/JA094iA03p02677, 1989.
931 McNutt, R. L., J. W. Belcher, J. D. Sullivan, F. Bagenal, and H. S. Bridge,
932 Departure from rigid co-rotation of plasma in jupiter's dayside
933 magnetosphere, *Nature*, *280* (5725), 803–803, doi:10.1038/280803a0,
934 1979.

935 Mendillo, M., J. Wilson, J. Spencer, and J. Stansberry, Io's volcanic control of
936 Jupiter's extended neutral clouds, *Icarus, 170*(2), 430–442,
937 doi:10.1016/j.icarus.2004.03.009, 2004.
938 Mendillo, M., S. Laurent, J. Wilson, J. Baumgardner, J. Konrad, and W. C. Karl,
939 The sources of sodium escaping from Io revealed by spectral high
940 definition imaging, *Nature, 448*(7151), 330–332, 2007.
941 Milillo, A., et al., Energetic neutral particles detection in the environment of
942 jupiter's icy moons: Ganymede's and europa's neutral imaging
943 experiment (genie), Planetary and Space Science, 88 (0), 53–63,
944 doi:10.1016/j.pss.2013.08.008, 2013.
945 Nakano, S., G. Ueno, Y. Ebihara, M.-C. Fok, S. Ohtani, P. C. Brandt, D. G.
946 Mitchell, K. Keika, and T. Higuchi, A method for estimating the ring
947 current structure and the electric potential distribution using energetic
948 neutral atom data assimilation, *J. Geophys. Res.*, *113* (A5),
949 doi:10.1029/2006JA011853, 2008.
950 Nozawa, H., H. Misawa, S. Takahashi, A. Morioka, S. Okano, and R. Sood,
951 Long-term variability of [SII] emissions from the io plasma torus
952 between 1997 and 2000, *J. Geophys. Res., 109*(A7), A07,209,
953 doi:10.1029/2003JA010241, 2004.
954 Orsini, S., A. Milillo, E. D. Angelis, A. M. D. Lellis, V. Zanza, and S. Livi,
955 Remote sensing of mercury's magnetospheric plasma environment via
956 energetic neutral atoms imaging, *Planet. Space Sci., 49* (14-15), 1659–
957 1668, 2001.
958 Orsini, S., S. Livi, K. Torkar, S. Barabash, A. Milillo, P. Wurz, A. M. Di Lellis,
959 and E. Kallio, Serena: A suite of four instruments (ELENA, STROFIO,
960 PICAM and MIPA) on board BepiColombo-MPO for particle detection
961 in the Hermean environment, *Planet. Space Sci.*, *58* (1–2), 166–181,
962 doi:10.1016/j.pss.2008.09.012, 2010.
963 Plainaki, C., A. Milillo, A. Mura, S. Orsini, and T. Cassidy, Neutral particle
964 release from europa's surface, Icarus, 210(1), 385–395, 2010.
965 Rees, M. H., *Physics and Chemistry of the Upper Atmosphere*, Cambridge
966 University Press, 1989.

967 Richards, P. G., J. A. Fennelly, and D. G. Torr, EUVAC: A solar EUV flux model
968 for aeronomic calculations, *J. Geophys. Res.*, *99* (A5), 8981–8992,
969 doi:10.1029/94JA00518, 1994.
970 Roelof, E., and D. Williams, The terrestrial ring current-from in situ
971 measurements to global images using energetic neutral atoms, Johns
972 Hopkins APL Technical Digest, 9, 144–163, 1988.
973 Saito, Y., J. A. Sauvaud, M. Hirahara, S. Barabash, D. Delcourt, T. Takashima,
974 and K. Asamura, Scientific objectives and instrumentation of Mercury
975 Plasma Particle Experiment (MPPE) onboard MMO, *Planet. Space Sci.*,
976 *58* (1–2), 182–200, doi:10.1016/j.pss.2008.06.003, 2010.
977 Sandel, B. R., and A. L. Broadfoot, Discovery of an Io-correlated energy source
978 for Io's hot plasma torus, *J. Geophys. Res.*, *87* (A4), 2231–2240,
979 doi:10.1029/JA087iA04p02231, 1982.
980 Sandel, B. R., and A. J. Dessler, Dual periodicity of the Jovian magnetosphere, *J.*
981 *Geophys. Res., 93*, 5487–5504, 1988.
982 Schaufelberger, A., et al., Scattering function for energetic neutral hydrogen
983 atoms off the lunar surface, *Geophys. Res. Lett.*, *38*, L22202,
984 doi:10.1029/2011GL049362, 2011.
985 Schmidtke, G., F. G. Eparvier, S. C. Solomon, W. K. Tobiska, and T. N. Woods,
986 The TIGER (thermospheric–ionospheric geospheric research) program:
987 Introduction, *Adv. Space Res.*, *37* (2), 194–198,
988 doi:http://dx.doi.org/10.1016/j.asr.2005.02.088, 2006.
989 Schneider, N. M., J. T. Trauger, J. K. Wilson, D. I. Brown, R. W. Evans, and D. E.
990 Shemansky, Molecular origin of Io's fast sodium, *Science*, *253* (5026),
991 1394–1397, doi:10.1126/science.253.5026.1394, 1991.
992 Schneider, N. M., and F. Bagenal, Io's neutral clouds, plasma torus,
993 magnetospheric interaction, in *Io After Galileo: A new view of Jupiter's*
994 *Volcanic Moon*, edited by R. M. C. Lopes and J. R. Spencer, pp. 265–
995 286, Springer, 2007.
996 Smyth, W. H., and M. R. Combi, A general model for Io's neutral gas clouds. I -
997 Mathematical description, *ApJ Suppl. Ser.*, *66*, 397–411,
998 doi:10.1086/191264, 1988.

999 Smyth, W. H., Neutral cloud distribution in the Jovian system, *Adv. Space Res.*,
1000 *12* (8), 337–346, 1992.
1001 Smyth, W. H., and M. Marconi, Nature of the iogenic plasma source in Jupiter's
1002 magnetosphere I. Circumplanetary distribution, *Icarus*, *166* (1), 85–106,
1003 doi:10.1016/S0019-1035(03)00176-3, 2003.
1004 Steffl, A. J., A. I. F. Stewart, and F. Bagenal, Cassini UVIS observations of the Io
1005 plasma torus: I. initial results, *Icarus, 172*(1), 78–90, doi:
1006 10.1016/j.icarus.2003.12.027, 2004a.
1007 Steffl, A. J., F. Bagenal, and A. I. F. Stewart, Cassini UVIS observations of the Io
1008 plasma torus: II. radial variations, *Icarus, 172*(1), 91–103, doi:
1009 10.1016/j.icarus.2004.04.016, 2004b.
1010 Steffl, A. J., P. A. Delamere, and F. Bagenal, Cassini UVIS observations of the Io
1011 plasma torus: III. observations of temporal and azimuthal variability,
1012 *Icarus, 180* (1), 124–140, doi:10.1016/j.icarus.2005.07.013, 2006.
1013 Steffl, A. J., P. A. Delamere, and F. Bagenal, Cassini UVIS observations of the Io
1014 plasma torus: IV. modeling temporal and azimuthal variability, *Icarus,*
1015 *194* (1), 153–165, doi: 10.1016/j.icarus.2007.09.019, 2008.
1016 Thomas, N., F. Bagenal, T. W. Hill, and J. K. Wilson, The Io neutral clouds and
1017 plasma torus, in *Jupiter: The Planet, Satellites and Magnetosphere*, chap.
1018 23, pp. 561–591, Cambridge University Press, 2004.
1019 Wang, K., R. M. Thorne, R. B. Horne, and W. S. Kurth, Cold torus whistlers: An
1020 indirect probe of the inner jovian plasma- sphere, *J. Geophys. Res. 103*,
1021 14 987-14 994, 1998a.
1022 vVang, K., R. l'vi. Thorne, R. B. Horne, and W. S. Kurth, Constraints on jovian
1023 plasma properties from a dispersion analysis of unducted whistlers in
1024 the warm Io torus, *J. Geophys. Res. 103*, 14 979-14 986, 1998b.
1025 Wieser, M., et al., Extremely high reflection of solar wind protons as neutral
1026 hydrogen atoms from regolith in space, *Planet. Space Sci.*, *57*, 2132–
1027 2134, doi:10.1016/j.pss.2009.09.012, 2009.
1028 Wilson, J., M. Mendillo, J. Baumgardner, N. Schneider, J. Trauger, and B. Flynn,
1029 The dual sources of Io's sodium clouds, *Icarus*, *157* (2), 476–489,
1030 doi:10.1006/icar.2002.6821, 2002.

Wurz, P., Detection of energetic neutral particles, in *The Outer Heliosphere: Beyond the Planets*, edited by K. Scherer, H. Fichtner, and E. Marsch, pp. 251–288, Copernicus Gesellschaft e. V., Katlenburg-Lindau, 2000.

Yoneda, M., M. Kagitani, and S. Okano, Short-term variability of jupiter's extended sodium nebula, *Icarus, 204*(2), 589–596, doi: 10.1016/j.icarus.2009.07.023, 2009.

Yoneda, M., H. Nozawa, H. Misawa, M. Kagitani, and S. Okano, Jupiter's magnetospheric change by Io's volcanoes, *Geophys. Res. Lett., 37*(11), L11,202, doi:10.1029/2010GL043656, 2010.

Yoneda, M., et al., Mid-infrared observations of Io's volcanism from the ground in 2011 and 2012, *Icarus, 236*, 153–156, doi: 10.1016/j.icarus.2014.01.019, 2014.

Zarka, P., J. Queninnec, and F. J. Crary, Low-frequency limit of jovian radio emissions and implications on source locations and Io plasma wake, *Planet. Space Sci. 49*, 1137-1149, 2001.

Appendix A: ENA flux calculation under the influence of a gravity field

The ENA flux, j_{ENA}[cm^{-2} s^{-1} sr^{-1} eV^{-1}] is normally calculated as a line-of-sight integral of ENA generation:

$$j_{\mathrm{ENA}}(E) = \int_{-\infty}^{0} j_{\mathrm{plasma}}(E, \hat{l}) \cdot N_n(l) \cdot \sigma \cdot dl \qquad \text{(A1)}$$

where, j_{plasma} denotes the differential flux of plasma, E is the energy, l is the distance along the direction of flight of the ENAs, and $\hat{l}$ is the unit vector thereof. N_n and σ are the density of the neutral atoms and the cross section for the charge-exchange process, respectively. Equivalently, one may use the velocity distribution function, f_{ENA} [s^3/m^6], for the following formulation:

$$f_{\mathrm{ENA}}(\vec{v}) = \int_{-\infty}^{0} f_{\mathrm{plasma}}(v, \hat{l}) \cdot N_n(l) \cdot \sigma \cdot dl \qquad \text{(A2)}$$

where v is the velocity vector of the ENAs and v is their speed. f_{plasma} is the velocity distribution function of the plasma. In the following, the Expression (A2) is preferentially applied because although the velocity distribution functions are conserved by the translation of reference frames in velocity space, the differential flux is not.

Expressions of (A1) and (A2) can be used under the following assumptions: 1. the change in energy and direction during the charge exchange is negligibly small, 2. there is no loss of ENAs during the flight, 3. the observer is stationary, and 4. the trajectories of the ENAs are straight. The first assumption is, in most of the higher energy range, satisfied for the LENA case. For low energy images (say <30 eV), one has to in theory modify the energy loss and directional change to calculate the ENA flux. Under this circumstance, due to the angular spread, the image will be more "blurred". It is also noted that this effect should be visible in the frame moving together with the target neutrals. In the Io tori imaging case, the observer (spacecraft) is moving with respective to the Io neutral torus, the blurring effect will be less significant. In addition, the main peak of the Io tori ENAs is >100 eV for S and O, we neglect the energy loss and the directional change. The second assumption is not trivially negligible, but it is insignificant for Io-tori imaging (see section 3.2). To satisfy the third assumption, one should properly compensate for the spacecraft velocity (to be discussed below). The final assumption may be violated in the case of the Io torus imaging. The trajectories of low-speed LENAs are bent by the gravity of Jupiter, so (A2) should be modified.

Because no centrifugal nor Corioli's forces contribute explicitly, an inertial frame is used for the formulation. Under a gravitational field, the ENA production should be assessed along a ballistic trajectory. For the spacecraft position $\vec{r}_0$ and ENA velocity $\vec{v}_0$ to be observed, the ENA trajectory, $L = L(\vec{r}_0,\vec{v}_0)$, can be derived uniquely from the integral (backward in time) of the Newtonian equation of motion.

Let us now consider a small path length, dl, at a distance of l along the trajectory L. The position ($\vec{r}_1$) and velocity ($\vec{v}_1$) at distance l are determined by integrating the Newtonian equation of motion. Both are functions of l, namely,

1093 $\vec{r}_1 = \vec{r}_1(l)$ and $\vec{v}_1 = \vec{v}_1(l)$. The time at *l* is also determined from the Newtonian
1094 equation of motion: $t_1 = t_1(l)$. Because the flying time of the ENA from the
1095 generation point to the spacecraft is typically several hours, which cannot be
1096 disregarded considering the time scale of the change in the environment
1097 (corotation is ~10 hours), the simulation must consider that ENA arriving at time
1098 t_0 are generated at different timing (t_1) along the ballistic trajectory depending on
1099 *l*. The ENA flux production, df_{ENA}, from this path length, d*l* ,is then

$$df_{\mathrm{ENA}}(\vec{r_1}, \vec{v_1}; t1) = f_{\mathrm{plasma}}(\vec{r_1}, \vec{v_1}; t1) \cdot \sigma \cdot N_n(\vec{r_1}; t_1) dl \qquad \text{(A3)}$$

1100

1101 All quantities should be calculated at time of t_1. We assume no energy loss
1102 during the charge exchange, namely, the source plasma velocity is also $\vec{v}_1$.
1103 According to the Liouville theorem, the distribution function along the
1104 orbit is conserved. Thus, the integration of (A3) over the distance *l* yields the
1105 total ENA flux along the trajectory *L*.

1106 $$f_{\mathrm{ENA}}(\vec{r}_0,\vec{v}_0;t_0=0) = \int \mathrm{d}f_{\mathrm{ENA}}(\vec{r}_1,\vec{v}_1;t_1) = \int_{-\infty}^{0} f_{\mathrm{plasma}}(\vec{r}_1,\vec{v}_1;t_1)\cdot\sigma\cdot N_n(\vec{r}_1;t_1)\mathrm{d}l \qquad \text{(A4)}$$

1107 Expression (A4) describes the ENA velocity distribution function. A
1108 spacecraft is typically moving in an inertial frame, so the spacecraft velocity
1109 should be considered. We define the spacecraft (SC) coordinate system that
1110 moves with the spacecraft velocity, $\vec{V}_{\mathrm{sc}}$. The velocities in the inertial ($\vec{v}$) and SC
1111 ($\vec{v}'$) frames are related as follows: $\vec{v}' = \vec{v} + \vec{V}_{\mathrm{sc}}$. The velocity distribution function
1112 does not depend on the frame of the reference: $f(\vec{r},\vec{v}) = f'(\vec{r}',\vec{v}')$. Thus, the ENA
1113 velocity distribution function observed at the spacecraft can be described as

1114 $$f'_{\mathrm{ENA}}(\vec{r}'_0 = 0,\vec{v}'_0;t=0) = f_{\mathrm{ENA}}(\vec{r}_0,\vec{v}_0;t=0)$$

1115 The differential flux to be observed can be derived from the velocity
1116 distribution function.

1117 $$j'_{\mathrm{ENA}}(\vec{r}'_0 = 0, E'_0, \Omega'_0) = \frac{2E'_0}{m^2} f'_{\mathrm{ENA}}(\vec{r}'_0 = 0, \vec{v}'_0) = \frac{2E'_0}{m^2} f_{\mathrm{ENA}}(\vec{r}_0, \vec{v}_0)$$

1118 Here, energy and direction (E_0', Ω'_0) can be calculated from $\vec{v}_0'$ (and vice
1119 versa), and *m* is the mass of ENAs. In the rightmost expression, the energy is
1120 given in the SC frame (E_0').
1121

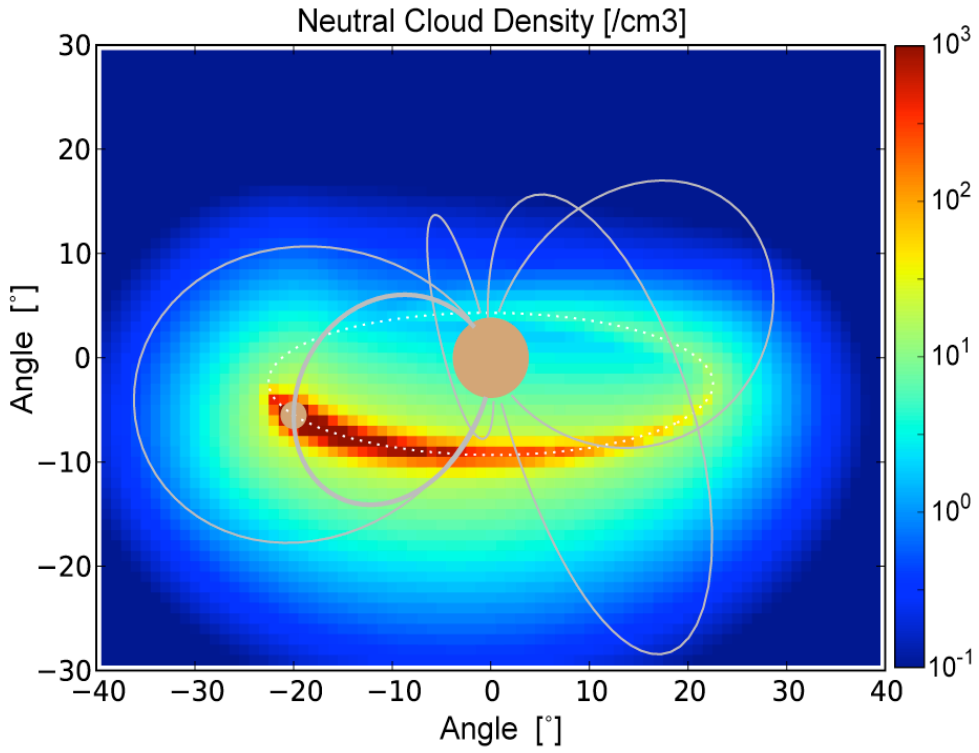

1122

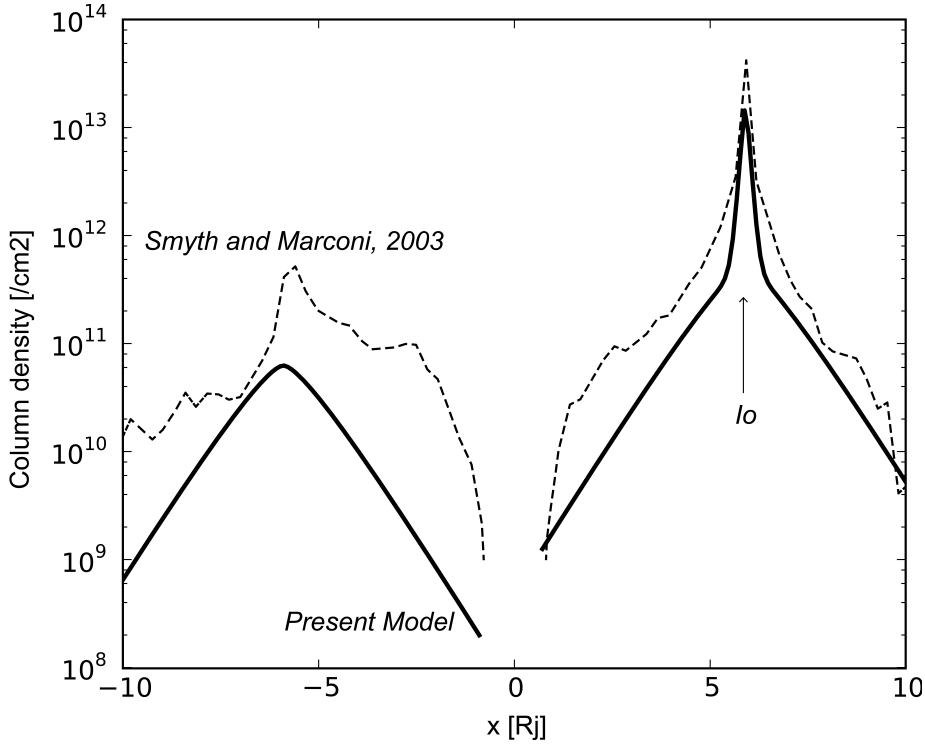

1123

1124

1125 ***Figure 1: a)*** *Image of the density model of the Io neutral torus used in this paper.*
1126 *A virtual spacecraft was placed at ~15 Rj from Jupiter. The spacecraft is above*
1127 *the equatorial plane at ~16° north. The dipole magnetic field lines (L=10) are*
1128 *shown as thin gray lines. The field line that is connected to Io (small circle; not*
1129 *to scale) is depicted with a thick line. Jupiter, located at the center, is drawn to*

scale. ***b)*** *Comparison of our model (thick line) and the result obtained by Smyth and Marconi (2003; dashed line). The column density integrated along the z-axis (perpendicular to the Io orbital plane) is shown as a function of the Jupiter-Io distance along the Jupiter-Io line.*

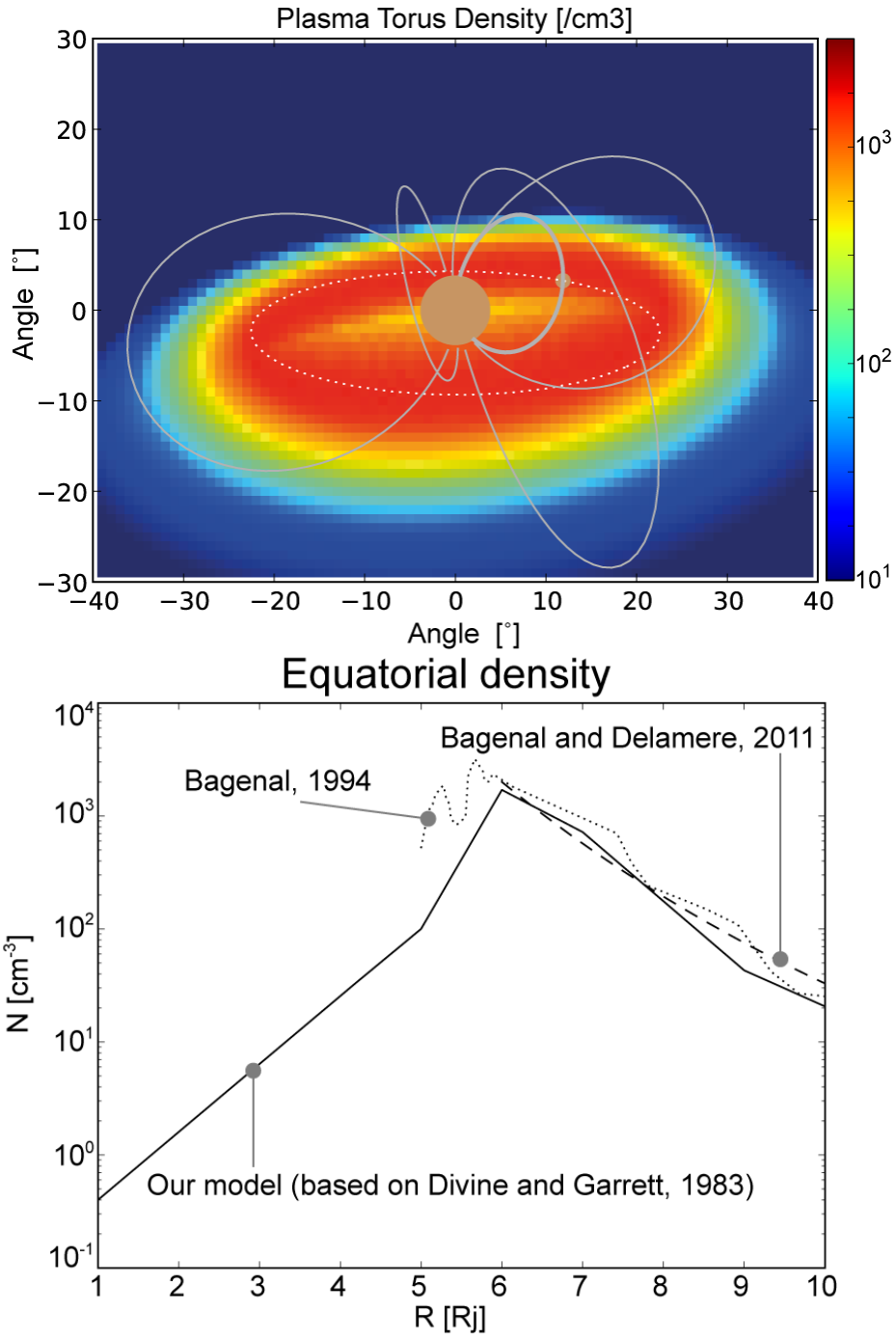

Figure 2: *a) Plasma density employed in the plasma-torus model in the same format as Figure 1a. b) The plasma density at the centrifugal equator as a function of the distance from the Jovian center. For comparison, two models (Bagenal,1994 and Bagenal and Delamere, 2011) are shown.*

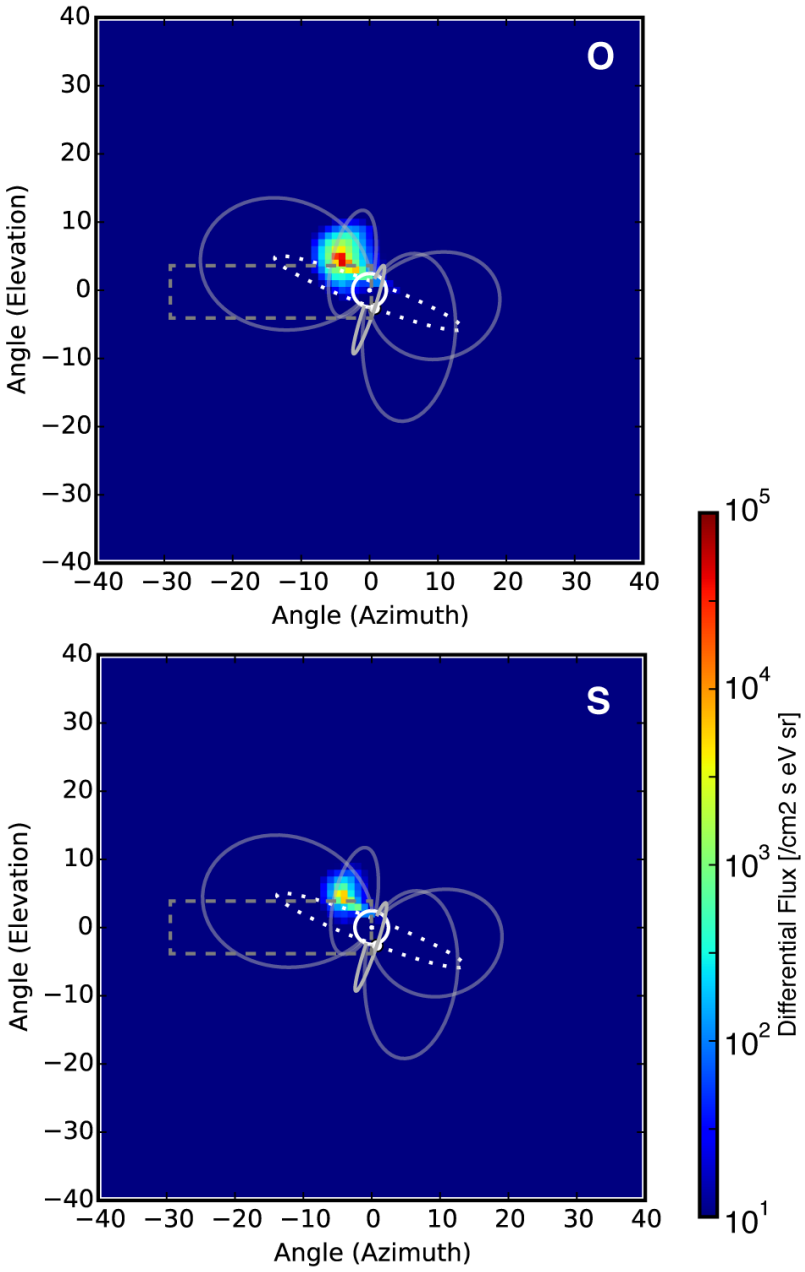

***Figure 3**: The expected oxygen and sulfur LENA images for an energy of 210 eV and 420 eV. The spacecraft was located at 23.3 Rj at a latitude of 6.5° north from the Jovian equatorial plane as an example. The spacecraft-Io-Jupiter line is nearly co-aligned in the projection plane (Jupiter equatorial plane). The open circle at the origin is Jupiter (to scale). The thin gray curves are Jupiter's magnetic field lines for L=10. The location of Io at the time of observation is indicated by the filled circle in front of Jupiter, but it is not to scale; the real size of Io is considerably smaller. The magnetic field line of Jupiter that crosses the body of Io is represented by the white curve. The dotted white circle*

corresponds to the Io orbit. The sensor's field of view (see Table 2), which is used for Figure 5, is indicated by the gray dotted rectangle.

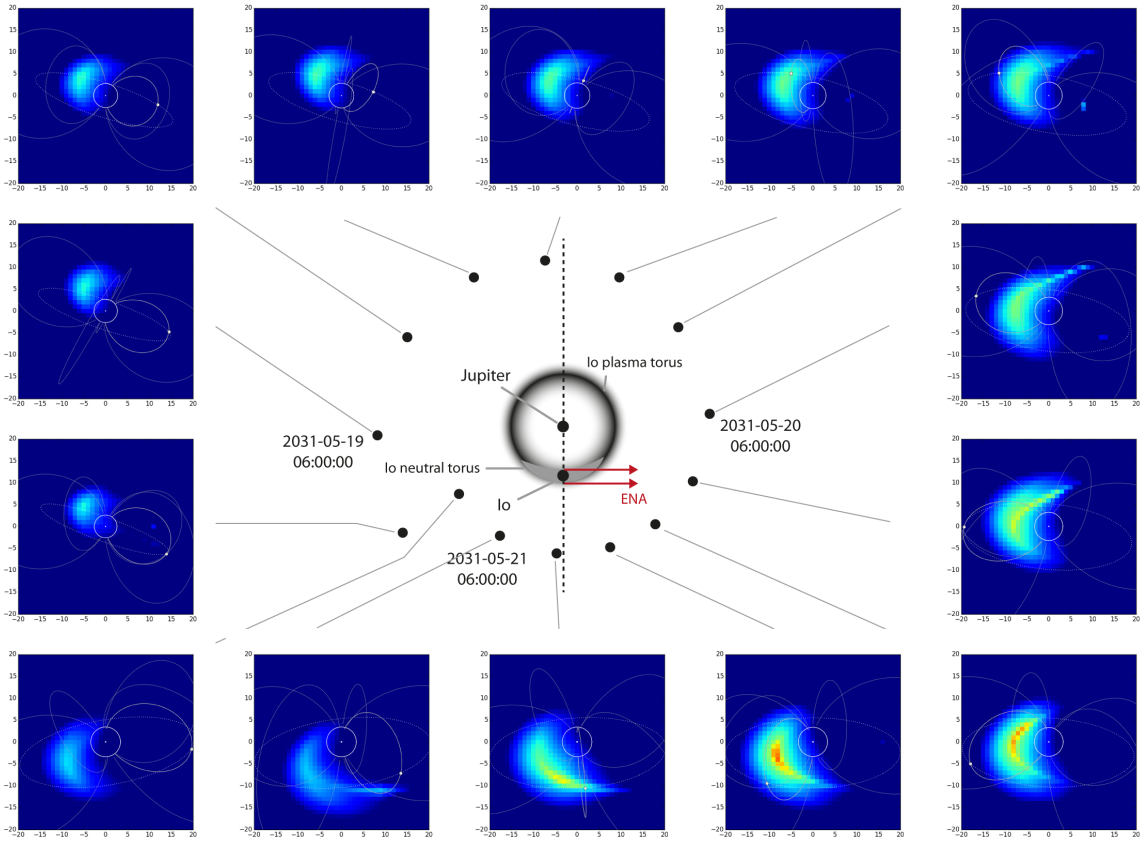

***Figure 4**: Time series of simulated oxygen LENA images with energy of 210 eV. Illustration at the center is the geometry of the calculation. The Jupiter-centered Io fixed frame is used. In this frame, the LENA is emitted always in the same direction (red arrows). Spacecraft location every 4 hours are depicted by filled dots. Each panel shows the LENA image in the same format as Figure 3, but zoomed into 20x20 degrees.*

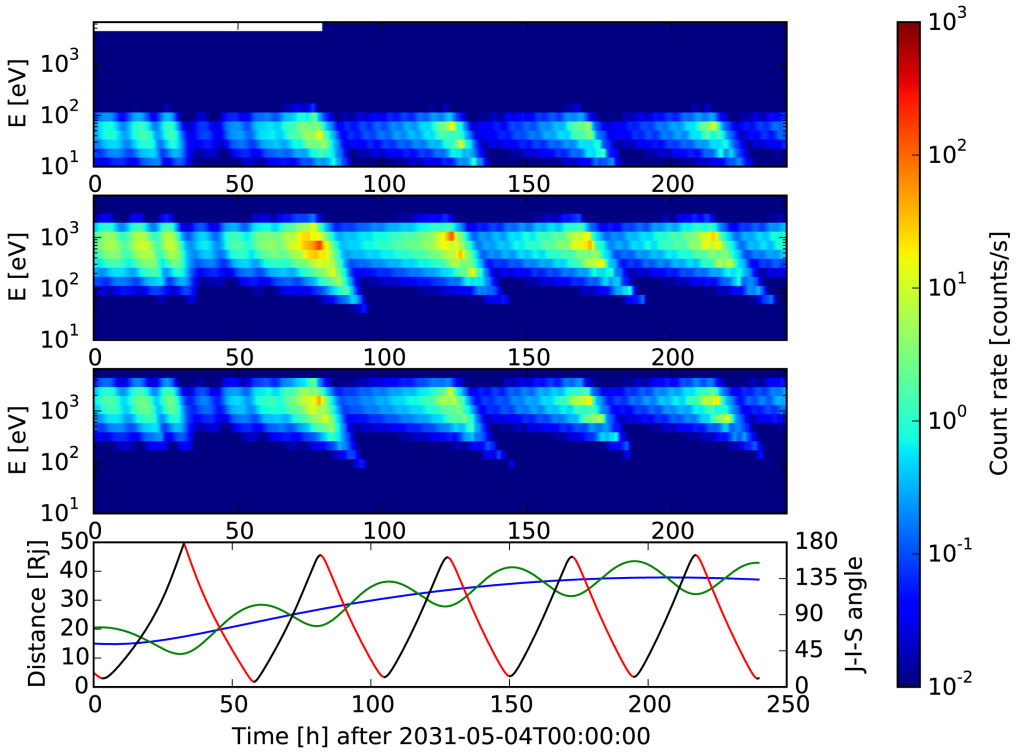

***Figure 5**: a-c) Calculated energy-time spectrograms for three species of LENAs (H, O, and S). The preliminary JUICE orbit and the geometric factor of the JNA-prototype are used to calculate the count rates. A sensor pixel of 30x5° is used (see white box in Figure 3). d) The geometry of the spacecraft, Io, and Jupiter. The blue and green solid lines are the distances of the spacecraft from Jupiter and Io, respectively. The black and red solid lines represent the Jupiter-Io-spacecraft angle. A black (red) line indicates that Io is located on the toward (away) side, as seen from the spacecraft.*

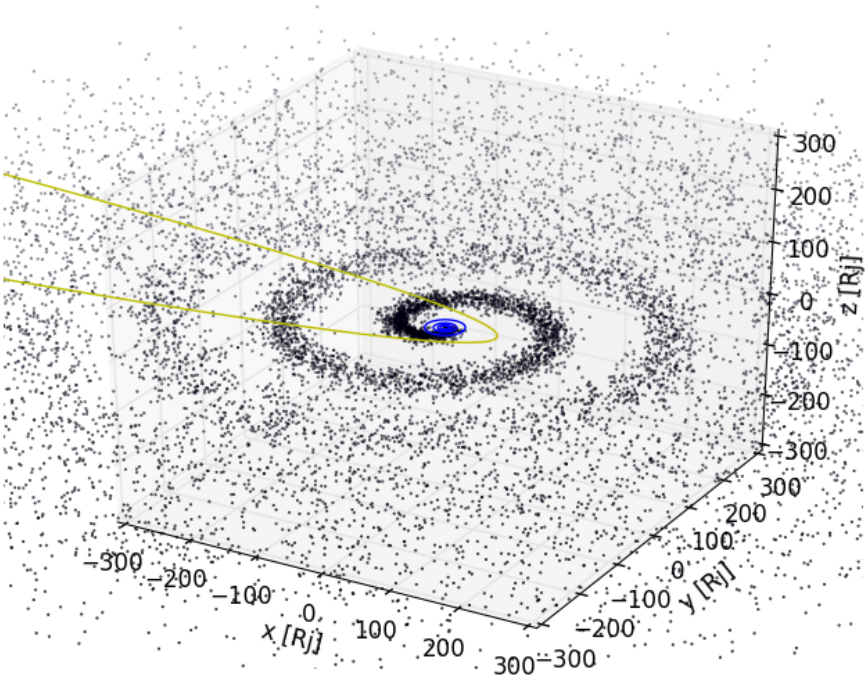

***Figure 6**: A snapshot of a 3-D view of the spatial distribution of LENAs from the Io torus. Each dot represents a charge-exchanged LENA. The four blue circles in the center correspond to the orbits of the Galilean moons (the innermost circle corresponds to Io). A very simplified shape of the Jovian magnetopause (in the equatorial plane of Jupiter) is shown for reference.*

Table 1*: Charge-exchange cross sections in the units of 10^{-16} cm^2 for each plasma species at a relative velocity of ~60 km/s. For hydrogen- and proton-related reactions, we refer to Lindsay and Stebbings (2005). For other reactions, data from McGrath and Johnson (1989) are used. The convolved cross section for each ion species are first calculated by taking the weighted average of the neutral species. Then, taking the weighted average the relative fraction of the parent ion species in different charge state, the total cross section for each LENA species are calculated. Reactions for which cross sections are unavailable are disregarded for the calculation of total cross sections.*

	H	O	S	O2	SO	SO2	Convolved cross section	Fraction	Total cross section
H+	39	11		10			11.8	0.1	11.8
O+	11	22	11.2	13	1.6	11	18.9	0.4	18.8
O++		9.86	39				14.1	0.01	
S+		0	29	0	50	0	5.2	0.1	8.8
S++		12.15	13.5				11.2	0.15	
Fraction	0.56	4	1	0	0	0			

1193 ***Table 2**: Specifications of the LENA sensor (JNA-prototype) used to calculate the*
1194 *count rate from the physical quantities. The parameters are based on the*
1195 *predecessor sensors of the JNA-prototype, namely, ENA, mounted on*
1196 *BepiColombo/MMO and CENA mounted on Chandrayaan-1 (Kazama et al.,*
1197 *2006; Barabash et al., 2009).*
1198

Angular resolution	30°x5°
Aperture	150°x7°
Energy range	10–3000 eV
Mass resolution	H, He, O, S, >S
Geometric factor (incl. efficiency)	5x10⁻ cm⁻ sr eV/eV
Energy resolution (DE/E)	100%

1199
1200

***Table 3**: Characteristic quantities that can be retrieved from Io-torus LENA imaging.*

	Absolute value	Short-term (abrupt) variation	Long-term variation
Plasma torus			
Density	Convolved (line of sight (LOS) integral)	Instantaneous relative (velocity distribution function (VDF) shape change)	With difficulty
Velocity		Instantaneous (LOS weighted)	
Temperature		Instantaneous (LOS weighted)	
Composition (Species)		Instantaneous (LOS weighted)	
Composition (Charge state)		Possibly instantaneous (via velocity distribution function?)	
Neutral torus			
Density	Convolved (LOS integral)	Instantaneous relative (VDF shape invariant)	With difficulty
Velocity		No	
Temperature		No	
Composition		No or with difficulty (via cross section?)	

1205